The high energy spectrum of NGC 4151

V. Beckmann[1], N. Gehrels, C. Shrader[2]
NASA Goddard Space Flight Center, Exploration of the Universe Division, Greenbelt, MD 20771, USA
beckmann@milkyway.gsfc.nasa.gov

S. Soldi
INTEGRAL Science Data Centre, Chemin d' Écogia 16, 1290 Versoix, Switzerland

P. Lubiński, A. A. Zdziarski
Nicolaus Copernicus Astronomical Center, Bartycka 18, 00-716 Warsaw, Poland

P.-O. Petrucci
Laboratoire d'Astrophysique de Grenoble, BP 53X, 38041 Grenoble Cedex, France
and

J. Malzac[3]
Centre d'Étude Spatiale des Rayonnements, 31028 Toulouse, France

ABSTRACT

We present first *INTEGRAL* observations of the type 1.5 Seyfert galaxy NGC 4151. Combining several *INTEGRAL* observations performed during 2003, totaling ~ 400 ksec of exposure time, allow us to study the spectrum in the 3 - 300 keV range. The measurements presented here reveal an overall spectrum from X-rays up to the soft gamma-rays that can be described by an absorbed ($N_{\rm H} \simeq 5 \times 10^{22}\,{\rm cm}^{-2}$) and non-variable thermal component, plus a Fe Kα line, and an exponential cutoff occurs at 110 keV, consistent with earlier claims. The Galactic hydrogen column density in the line of sight is $N_{\rm H,Gal} \simeq 2.1 \times 10^{20}\,{\rm cm}^{-2}$. The time resolved analysis shows little variation of the spectral parameters. The comparison with *CGRO*/OSSE data shows that the same spectral model can be applied over a time span of 15 years, while the flux varied by a factor of 2. Applying a Compton reflection component improves the model fit to the *INTEGRAL* data. Nonetheless the data available to date cannot significantly confirm or exclude the existence of reflection, nor is a high iron overabundance in the absorber, as had been previously suggested, clearly detectable.

Subject headings: galaxies: active — galaxies: individual (NGC 4151) — gamma rays: observations — X-rays: galaxies — galaxies: Seyfert

[1]also with the Joint Center for Astrophysics, Department of Physics, University of Maryland, Baltimore County, MD 21250, USA

[2]also with Universities Space Research Association

[3]also with the Institute of Astronomy, University of Cambridge, Madingley Road, Cambridge CB3 0HA, United Kingdom

1. Introduction

The Seyfert galaxy NGC 4151 is one of the most intensly studied AGN (Active Galactic Nucleus). This is due to the fact that it is one of the apparently brightest ($V \simeq 11$ mag, bolometric luminosity $\sim 10^{44}\,\mathrm{erg\,s^{-1}}$) and nearest (16.5 Mpc for $H_0 = 75\,\mathrm{km\,s^{-1}}$) among its class. Observations throughout the electromagnetic spectrum revealed a complex and somewhat special case of a Seyfert 1.5 galaxy (see e.g. Dermer & Gehrels (1995) and Ulrich (2000) for a general review). In the optical the host galaxy appears to be a large barred spiral with nearly face-on orientation, showing two thin spiral arms (Arp 1977). In the high-energy domain, NGC 4151 has been studied by various X-ray missions. Here the AGN shows a relatively hard spectrum with a photon index Γ which varies between 1.4 and 1.7. The spectrum seems to be best described by a power law with an exponential cut-off at > 50 keV and an iron fluorescence Kα line at 6.4 keV (Piro 1999; Piro et al. 2000). In addition to the fluorescence line, which reveals the existence of cooler material surrounding the AGN, a reflection hump in the 10 – 30 keV has been reported in Ginga/OSSE data (Zdziarski et al. 1996) and in *BeppoSAX* data (Petrucci et al. 2001; Schurch & Warwick 2002).

In this paper we present analysis of recent observations of NGC 4151 performed by the INTEGRAL satellite, and compare the results with previous studies.

2. Simultaneous optical, X-ray and gamma-ray observations

Observations in the X-ray to soft gamma-ray domain have been performed in late May 2003 by the *INTEGRAL* satellite (Winkler et al. 2003). This mission offers the unique possibility to perform simultaneous observations over the 2 – 8000 keV energy region. This is achieved by the X-ray monitor (2–30 keV) JEM-X (Lund et al. 2003), the soft gamma-ray imager (20–1000 keV) ISGRI (Lebrun et al. 2003), and the spectrograph SPI (Vedrenne et al. 2003), which operates in the 20 – 8000 keV region. In addition to these data an optical monitor (OMC, Mas-Hesse et al. 2003) provides photometric measurements in the V band.

In order to extend the spectral coverage, we use data from *RXTE*.

2.1. *INTEGRAL* data

For the analysis of the high energy spectrum of NGC 4151 we used the data which were taken within 10 degrees radius around the source. The journal of observations is shown in Tab. 1. The exposure times were taken from the ISGRI effective on-source times. This value is approximately the same for the spectrograph SPI, but for the JEM-X and OMC monitors it has to be taken into account that they cover a much smaller sky area. Thus in the case of dithering observation, the source is not always in the field of view of the monitors. The analysis was performed using version 4.2 of the Offline Science Analysis (OSA) software distributed by the ISDC (Courvoisier et al. 2003b).

NGC 4151 was too faint above ~ 150 keV to be seen by IBIS/PICsIT. Summing all available *INTEGRAL* data together shows that NGC 4151 is detected within the exposure time of 408 ksec up to 300 keV. No intercalibration had to applied between JEM-X and ISGRI, but the SPI data appear to be at a higher level by a factor of 1.3. The SPI data further show some energy bins where the reconstruction software SPIROS (Skinner & Connell 2003) could not find a solution, and others which indicate problems in the background subtraction. This is not surprising as most of the data have been taken in staring mode, which is known to cause problems in the SPI analysis, because the background level cannot be determined (Dubath et al. 2005).

The ISGRI spectra have been extracted using the standard method. Concerning the calibration of the data it has to be taken into account that the response of ISGRI is still not well known, even though this would be more severe for off-axis observations. The spectra of the Crab taken with JEM-X show systematic features in the 5 – 7 keV energy range, which might affect the measurement of the iron Kα line.

2.2. *RXTE* data

The All Sky Monitor (ASM) on board the Rossi X-ray Timing Explorer (*RXTE*) scans about 80% of the sky every orbit. This offers a unique way to monitor the emission of bright X-ray sources like NGC 4151 in the 1.5 – 12 keV energy range. We extracted fluxes from the *RXTE*/ASM data base. The fluxes have been averaged over one day

(see the triangles in Fig. 1). The data show a 10 ± 3 mCrab flux over the duration of the *INTEGRAL* observations.

2.3. *CGRO* data

The source was also monitored in the $\sim 20 - 100$ keV band by the *CGRO*/BATSE experiment from 1991-2000 (Parsons et al. 1998; Harmon et al. 2004). Those measurements are made using an Earth-occultation technique, and are thus sampled one time per 90 min *CGRO* orbit. In practice, NGC 4151 is a faint source for that instrument, but daily summations lead to $\sim 3\sigma$ determinations. We obtained the BATSE data spanning the ~ 3.5 yr overlap of the *RXTE* and *CGRO* missions, for the purpose of monitoring the long-term hard-to-soft spectral behavior.

3. X-ray to Gamma-ray spectrum

3.1. Time Averaged Spectral Analysis

The overall spectrum extracted from the *INTEGRAL* JEM-X and ISGRI data is shown in Fig. 2. A systematic error of 3% has been added to the ISGRI and SPI data. The fit results however do not depend on the SPI data, which do not influence any model fit because of the larger error bars compared to the ISGRI data in the same energy region.

The spectral fitting was done using version 11.3.1 of XSPEC (Arnaud 1996). The data in the range $3 - 300$ keV are well represented by a rather simple model. We applied a fit of an absorbed power law with an exponential high-energy cut-off, and added a Gaussian line in order to account for the iron Kα fluorescence line. The best fit values are $\Gamma = 1.52^{+0.04}_{-0.04}$, $E_C = 109^{+15}_{-12}$ keV, and $N_{\rm H} = 5.08^{+0.68}_{-0.66} \times 10^{22}\,{\rm cm}^{-2}$. The fluorescence line shows an equivalent width of $EW = 119$ eV and a flux of $f_{{\rm K}\alpha} = 4.5^{+1.3}_{-1.6} \times 10^{-4}\,{\rm ph\,cm^{-2}\,s^{-1}}$ (all errors are 90% confidence values). The statistics do not allow us to see any effects of relativistic broadening of the iron line (see e.g. Yaqoob et al. 1995). The source had an average flux of $f_{20-200\,{\rm keV}} = 0.012\,{\rm ph\,cm^{-2}\,s^{-1}} = 9.6 \times 10^{-10}\,{\rm erg\,cm^{-2}\,s^{-1}}$. This model gives $\chi^2_\nu = 1.46$ for 189 degrees of freedom. The model of an absorbed power law without a cut-off leads to a significantly poorer fit result ($\chi^2_\nu = 1.9$).

Using a more complicate model by adding reflection from cold material to the cut-off power-law (the so-called PEXRAV model; Magdziarz & Zdziarski 1995) improves the fit. From radio measurements the inclination angle of the accretion disk is estimated to be $i \sim 65°$ (Pedlar et al. 1993). The free parameters in the PEXRAV model then are best fitted with a photon index of $\Gamma = 1.86^{+0.09}_{-0.09}$, a hydrogen column density of $N_{\rm H} = 7.0^{+0.8}_{-0.8} \times 10^{22}\,{\rm cm}^{-2}$, a folding energy of $E_{fold} = 414^{+738}_{-174}$ keV and a relative reflection of $R = 1.04^{+0.37}_{-0.31}$. The large uncertainty and high value of the folding energy outside the energy range covered by the spectrum indicates that the reflection component in total is not well constrained. The PEXRAV model leads to $\chi^2_\nu = 1.19$ for 188 degrees of freedom.

Another physically meaningful model describing Comptonization of soft photons by a hot plasma, the so called compTT model, has been developed by Titarchuk (1994). The model includes the plasma temperature T_e of the hot corona, the optical depth τ of this plasma, and the temperature T_0 of the soft photon spectrum. Because the spectrum starts at 2 keV, T_0 is not well constrained by the data and has been fixed to 10 eV. The model fit resulted in $N_{\rm H} = 6.5^{+0.5}_{-0.7} \times 10^{22}\,{\rm cm}^{-2}$, $kT_e = 35.8^{+6.7}_{-5.9}$ keV, and $\tau = 1.41^{+0.31}_{-0.24}$ for plane geometry. The compTT model gives $\chi^2_\nu = 1.58$ for 189 degrees of freedom, which is significantly worse than the PEXRAV model.

3.2. Spectral Evolution

In order to study the evolution of the spectrum in time, we applied ten time bins over the total observation period, combining about 33 ksec of effective on-time in each bin. We used only those data for which we have simultaneous JEM-X and ISGRI coverage. We then applied the cutoff power-law model to the single time bins and extracted fluxes in the $5 - 20$ keV and $20 - 100$ keV energy bin. The results are shown in Fig. 1. No significant variation of the flux can be seen here, and also the fit parameters are consistent over the observed period within the error bars. In order to look for variability on shorter time scales we then binned the *INTEGRAL* JEM-X2 and ISGRI data into 2000 sec time intervals (Fig. 3). Both lightcurves

show a minor outburst at $t \simeq 1243.0\,\mathrm{IJD}$[1]. An analysis of the enclosing time bin $1242.5\,\mathrm{IJD} < t < 1243.5\,\mathrm{IJD}$ does show a slightly increased flux ($f_{20-200\,\mathrm{keV}} = 0.0132\,\mathrm{ph\,cm^{-2}\,s^{-1}} = 1.03 \times 10^{-9}\,\mathrm{erg\,cm^{-2}\,s^{-1}}$) but the same spectral parameters.

For the same time intervals as used in the high-energy analysis, optical photometry values from the OMC have been extracted. Due to the high signal-to-noise these data have been binned into 1000 s time intervals (Fig. 4). The minimum in the optical lightcurve around $t \simeq 1243.0$ coincides with the maximum in the X-ray lightcurve. Because of the short time coverage of the observation it is not clear whether this is a coinincidence or a physical correlation between the optical and the hard X-ray domain.

3.3. Search for γ-ray line emission

The SPI spectrometer offers the opportunity to look for narrow line features. In case the high energy spectrum would be dominated by non-thermal processes, one could expect a significant amount of $e^{\pm}$ pair annihilation processes around 511 keV. At this energy, SPI has a resolution of $FWHM = 1.95\,\mathrm{keV}$ (Attié et al. 2003). *CGRO*/OSSE was able to determine the 3σ upper limit of a broad ($450 - 600\,\mathrm{keV}$) emission line feature with $f < 6 \times 10^{-5}\,\mathrm{ph\,cm^{-2}\,s^{-1}}$. We therefore looked for a comparably narrow feature by extracting an image in the $499 - 519\,\mathrm{keV}$ energy band, centred on the 511 keV rest-frame energy at NGC 4151's redshift. No emission at the restframe energy of the annihilation line is detectable. The 3σ upper limit extracted from the SPI data by SPIROS is $f_{499-519keV} = 10^{-4}\,\mathrm{ph\,cm^{-2}\,s^{-1}}$. The 3σ line sensitivity derived from ground calibration gives a similar value of $6.5 \times 10^{-5}\,\mathrm{ph\,cm^{-2}\,s^{-1}}$ (Roques et al. 2003). The measurement presented here is therefore not improving the *CGRO*/OSSE upper limit, because of the much shorter *INTEGRAL*/SPI exposure time.

4. Discussion

The *INTEGRAL* overall spectrum can be modelled by a rather simple absorbed cut-off power law plus an iron Kα fluorescence line. The more physical meaningful model of Comptonization of soft photons in a hot plasma gives a slightly better fit statistic, and shows that those circumstances are applicable to the case of NGC 4151.

The best comparable coverage in the energy range studied by *INTEGRAL* ISGRI and SPI has been provided by *CGRO*/OSSE (Johnson et al. 1997). The measurements from *INTEGRAL* and OSSE are compared in Tab. 2. The OSSE results have been derived by fitting simultaneously the individual OSSE spectra, allowing for different normalisation. Our results are similar to what has been reported in Johnson et al. (1997). We compared the OSSE data directly with the *INTEGRAL* observation through simultaneous fitting. Figure 5 shows a simultaneous fit of both data sets, the average *INTEGRAL* and average *CGRO*/OSSE spectrum. The data are well represented by a cutoff power law with individual constant factors in order to account for flux variability ($\chi^2_\nu = 1.18$). Note that the energy range above $\sim 100\,\mathrm{keV}$ is dominated by the OSSE data, as their error bars are significantly smaller than the *INTEGRAL* ones. This is because the *INTEGRAL* exposure time is much smaller. The fit shows that the 20-200 keV flux varied by a factor of 2 over the individual *INTEGRAL* and *CGRO* observations. It is remarkable that the same simple model with $\Gamma = 1.5$ and $E_C = 100\,\mathrm{keV}$ represents well the data from the different *CGRO*/OSSE and *INTEGRAL* observations.

When applying the PEXRAV model to the *CGRO* data it turns out that a reflection component is not required. This is not surprising, as there are no OSSE data below 50 keV where a reflection component would have a significant influence. The PEXRAV fit to the combined data shows that a reflection component is also not required by the data. The reduced χ^2 is similar to that of the cutoff power law, and the fit result is consistent with no reflection ($R = 0$) at a 2σ level.

This is mainly consistent with previous *BeppoSAX* observations. Three observations by *BeppoSAX*, two in 1996 and one in 1999, show that a reflection component is not required in most cases with $R_{1996H} = 0.01, R_{1999} = 0.2$, and $R_{1996L} = 0.45$ (Petrucci et al. 2001). In the latter case the fit resulted in a large optical depth τ, indicating that a reflection component, if present, would be

[1] IJD is related to the modified Julian Date by $IJD = MJD - 51544.0$

smeared out over a wide energy range making its existence more difficult to prove.

Another study of the high energy spectrum of NGC 4151 combining *CGRO*/OSSE and ASCA data has been presented by Zdziarski et al. (2002). This work also came to the conclusion that the data can be represented by a simple cut-off power law with a narrow iron Kα line, adding thermal bremsstrahlung at low energies, which are not covered by our data. This fit resulted in a $\chi^2_\nu = 1.6$ and the authors added a broad Gaussian line in order to account for residuals in the $5 - 6.5\,\mathrm{keV}$ energy band. Zdziarski et al. argue that a model with complex absorption and Compton reflection component is more likely to give a physical meaningful explanation for the observed spectrum. They also argue that the absorber in NGC 4151 shows evidence for the presence of several absorbing components in the line of sight, which cannot be confirmed by our data, mainly because of the lack of data below 2 keV.

Matt et al. (2003) argue that absorption in Seyfert 2 galaxies can be caused by several circumnuclear regions. They favour a model with a possible temporary switching-off of the nuclear radiation to explain observed variability. Their model predicts an iron Kα equivalent width of $\sim 100\,\mathrm{eV}$ for a Compton thick case with $N_\mathrm{H} \simeq 10^{23}\,\mathrm{cm}^{-2}$, consistent with our measurements for NGC 4151. This could mean that the iron line could be produced in material in the line of sight, with large distance to the central engine of the AGN.

Schurch & Warwick (2002) showed that the same 'template' spectrum matches observations of NGC 4151 done by ASCA, BeppoSAX and even XMM-Newton (Schurch et al. 2003). Their model spectrum includes a strong reflection component ($R \simeq 2$ from PEXRAV) as well as an absorption component with variable iron abundance. When we apply this to the *INTEGRAL* data with the simple cutoff powerlaw and leave the iron abundance variable, we also detect an enhanced iron abundance by a factor of $2.3^{+2.8}_{-2.8}$, and get an improved fit result ($\chi^2_\nu = 1.33$ instead of $\chi^2_\nu = 1.46$). In this manner we are able to model the high-energy spectrum in a simple way without the need of any reflection component. The large error on the iron abundance indicates though that the data cannot put significant constrains on the true abundance in the absorbing material. The effect on the χ^2_ν shows that additional components, like a variable abundance or a reflection component, can improve the fit statistics, but may not lead to improved insight on the physical conditions in the source.

Most Seyfert galaxies show a softening of the X-ray continuum as sources brighten (Markowitz, Edelson, & Vaughan 2003; Nandra et al. 1997). We did not see significant variations of the spectral parameters over the duration of our observations. Especially, we did not detect any correlation of flux with spectral slope. This can be understood when studying the correlation of spectral hardness ratio with flux as derived from simultaneous *CGRO*/BATSE and *RXTE*/ASM data as shown in Fig. 6. Here we have plotted the hardness ratio $(20 - 100\,\mathrm{keV})/(2 - 12\,\mathrm{keV})$ versus the RXTE $(2 - 12\,\mathrm{keV})$ flux based on daily averages from 1996-2000. An overall correlation is discernible, but the scatter is large and thus might not be detectable over a time span of 400 ksec (as in our case), and can even be missed when comparing the long-term observations by *CGRO*/OSSE.

5. Conclusion

The results from the *INTEGRAL* JEM-X2, ISGRI, and SPI data show that the high-energy spectrum of NGC 4151 can be approximated by a rather simple model. The spectrum above 2 keV is described by an absorbed ($N_\mathrm{H} = 5.1 \times 10^{22}\,\mathrm{cm}^{-2}$) cut-off ($E_C = 110\,\mathrm{keV}$) power law ($\Gamma = 1.5$) with a narrow iron K$\alpha$ line ($EW = 119\,\mathrm{eV}$). A Compton reflection model (PEXRAV) gives a significantly better fit result with $\Gamma = 1.86^{+0.09}_{-0.09}$, a hydrogen column density of $N_\mathrm{H} = 7.0^{+0.8}_{-0.8} \times 10^{22}\,\mathrm{cm}^{-2}$, a folding energy of $E_{fold} = 410^{+740}_{-170}\,\mathrm{keV}$ and a relative reflection of $R = 1.04^{+0.37}_{-0.31}$. However, this latter result is questionable as the inferred E_{fold} parameter is clearly not constrained by our data.

The comparison to previous *CGRO*/OSSE measurements shows that the simpler cut-off power law model is a valid representation of the high energy spectrum over decadal timescales, when applying a different normalisation to the various observations. A significant variation of the spectral parameters during the *INTEGRAL* observation cannot be detected. The effect of spectral softening with higher flux values can only be seen in observations covering longer time scales. This is

shown in the comparision of *CGRO*/BATSE (20–200 keV) to *RXTE*/ASM (2–10 keV) fluxes.

The *INTEGRAL* data cannot confirm the existence of a high iron overabundance in the absorber.

This is not to say that we claim that Compton reflection is not taking place in NGC 4151, but at the time of our observations, with the given data in the high energy range, we are not able to reach a conclusive result. The thermal Comptonization is clearly seen in the cutoff of the spectrum, ruling out non-thermal emission being dominant in this source. This is also confirmed by the non-detection of emission in the annihilation line in NGC 4151.

The study of NGC 4151 indeed shows that the *INTEGRAL* mission can give valuable insights on the characteristics of the high-energy cut-off in bright AGN, as has been already shown for the Seyfert 2 NGC 4388 (Beckmann et al. 2004a, 2004b). This shows that AGN can be well described by an optical thick disk with a hot corona. We will present a general overview on the properties of AGN observed by *INTEGRAL* in an upcoming paper.

This research has made use of the NASA/IPAC Extragalactic Database (NED) which is operated by the Jet Propulsion Laboratory and of data obtained from the High Energy Astrophysics Science Archive Research Center (HEASARC), provided by NASA's Goddard Space Flight Center.

REFERENCES

Arnaud, K.A. 1996, in: Astronomical Data Analysis Software and Systems V, eds. Jacoby G. and Barnes J., p17, ASP Conf. Series 101

Arp, H. C. 1977, ApJ, 218, 70

Attié, D., et al. 2003, A&A, 411, L71

Beckmann, V., Gehrels, N., Favre, P., Walter, R., Courvoisier, T. J.-L., Petrucci, P.-O., 2004, Malzac, J., ApJ, 614, 641

Beckmann, V., Gehrels, N., Favre, P., Courvoisier, T. J.-L., Walter, R., Malzac, J., Petrucci, P.-O., 2004, in: Proc. 5th INTEGRAL Workshop, ESA SP-552

Bianchi, S., Balestra, I., Matt, G., Guainazzi, M., Perola, G. C. 2003, A&A, 402, 141

Courvoisier, T.J.-L., et al. 2003a, A&A, 411, L343

Courvoisier, T.J.-L., et al. 2003b, A&A, 411, L53

Dermer, C. D., & Gehrels, N. 1995, ApJ, 447, 103

Dubath, P., et al. 2005, MNRAS, 357, 420

Harmon, B. A., et al. 2004, ApJS, 154, 585

Johnson, W. N., McNaron-Brown, K., Kurfuss, J. D., Zdziarski, A. A., Magdziarz, P., Gehrels, N., 1997, ApJ, 482, 173

Lebrun, F., et al. 2003, A&A, 411, L141

Lund, N., et al. 2003, A&A, 411, L231

Magdziarz, P., & Zdziarski, A. A. 1995, MNRAS, 273, 837

Malzac, J., & Petrucci, P.-O. 2002, MNRAS, 336, 1209

Markowitz, A., Edelson, R., & Vaughan, S. 2003, ApJ, 598, 935

Mas-Hesse, J. M., et al. 2003, A&A, 411, L261

Matt, G., Matteo, G., & Maiolino, R. 2003, MNRAS, 342, 422

Nandra, K., George, I. M., Mushotzky, R., Turner, T. J., & Yaqoob, T. 1997, ApJ, 476, 70

Parsons, A. M., Gehrels, N., Paciesas, W. S., Harmon, B. A., Fishman, G. J., Wilson, C. A., Zhang, S. N. 1998, ApJ, 501, 608

Pedlar, A., et al. 1993, MNRAS, 263, 471

Petrucci, P. O., et al. 2001, ApJ, 556, 716

Piro, L. 1999, AN, 320, 236

Piro, L. 2000, Adv. Space Res., 25, 453

Raymond, J. C., & Smith, B. W. 1977, ApJS, 35, 419

Roques, J. P., et al. 2003, A&A, 411, L91

Schurch, N. J., & Warwick, R. S. 2002, MNRAS, 334, 811

Schurch, N. J., Warwick, R. S., Griffiths, R. E., Sembay, S. 2003, MNRAS, 345, 423

Skinner, G., & Connell, P. 2003, A&A, 411, L123

Titarchuk, L. 1994, ApJ, 434, 570

Ulrich, M.-H. 2000, A&AR, 10, 135

Vedrenne, G., et al. 2003, A&A, 411, L63

Winkler, C., et al. 2003, A&A, 411, L1

Yaqoob, T., Edelson, R., Weaver, K. A., Warwick, R. S., Mushotzky, R. F., Serlemitsos, P. J., & Holt, S. S. 1995, ApJ, 453, L81

Zdziarski, A. A., Johnson, W. N., Magdziarz, P. 1996, MNRAS, 283, 193

Zdziarski, A. A., Leighly, K. M., Matsuoka, M., Cappi, M., Mihara, T. 2002, ApJ, 573, 505

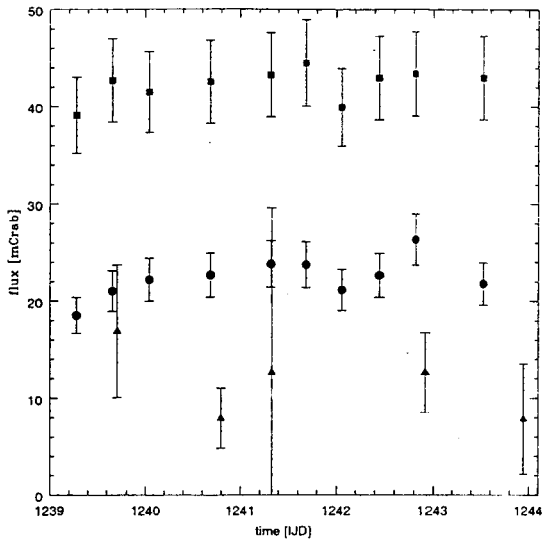

Fig. 1.— *INTEGRAL* and *RXTE*/ASM light curves in Crab units. The squares and circles represent the 20−100 keV ISGRI and 5−20 keV JEM-X2 lightcurve, respectively. Fluxes were extracted from model fits to the data. The triangles are *RXTE*/ASM 1.5 − 12 keV daily averages.

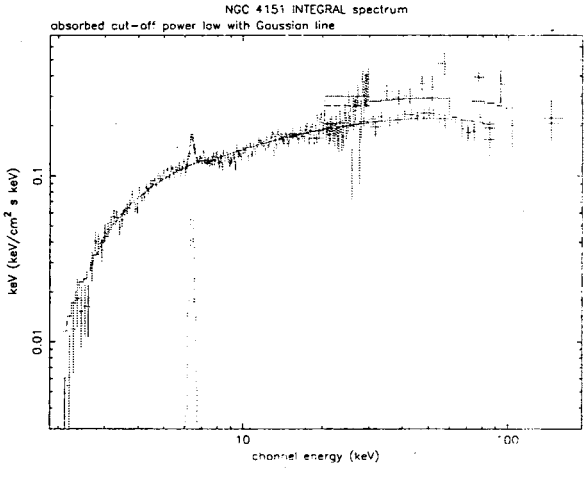

Fig. 2.— Summed spectrum of the *INTEGRAL* JEM-X2, ISGRI, and SPI data. The data are well represented by an absorbed exponential cut-off power law with $E_C = 109$ keV and photon index $\Gamma = 1.52$. In addition a gaussian iron Kα line with equivalent width $EW = 119$ eV appears in the spectrum.

This 2-column preprint was prepared with the AAS LaTeX macros v5.2.

Table 1: *INTEGRAL* observations

obs. date start	*INTEGRAL* revolution	exposure time [ksec]	number of pointings	observation mode
22/05/03	73	7.3	3	5×5
23/05/03	74	170.8	10	5×5, staring
25/05/03	75	174.5	5	staring
28/05/03	76	55.1	4	staring

Table 2: Spectral fits to average *INTEGRAL* and OSSE spectra

Model	Mission	Photon Index	E_C or kT [keV]	τ or R	$\chi^2_\nu(dof)$
Power law	*INTEGRAL*	$1.76^{+0.02}_{-0.02}$	...	...	1.90 (207)
Power law	*CGRO*/OSSE	$2.55^{+0.03}_{-0.03}$	...	...	1.73 (279)
PL-exp	*INTEGRAL*	$1.52^{+0.04}_{-0.04}$	109^{+15}_{-12}	...	1.46 (189)
PL-exp	*CGRO*/OSSE	$1.47^{+0.15}_{-0.16}$	90^{+16}_{-12}	...	0.98 (278)
PL-exp	*INTEGRAL*+*CGRO*	$1.49^{+0.04}_{-0.04}$	93^{+5}_{-5}	...	1.18 (469)
Thermal Comptonization[a]	*INTEGRAL*	...	36^{+7}_{-6}	$1.41^{+0.31}_{-0.24}$	1.58 (189)
Thermal Comptonization[a]	*CGRO*/OSSE	...	44^{+6}_{-5}	$0.89^{+0.18}_{-0.17}$	0.99 (277)
PEXRAV	*INTEGRAL*	$1.86^{+0.09}_{-0.09}$	410^{+740}_{-170}	$1.04^{+0.37}_{-0.31}$	1.19 (188)
PEXRAV	*CGRO*/OSSE	$1.52^{+0.25}_{-0.28}$	94^{+30}_{-9}	$0.00^{+2.78}_{-0.00}$	0.99 (276)
PEXRAV	*INTEGRAL*+*CGRO*	$1.62^{+0.07}_{-0.07}$	123^{+23}_{-17}	$0.41^{+0.23}_{-0.20}$	1.14 (468)

[a] Following Titarchuk 1994

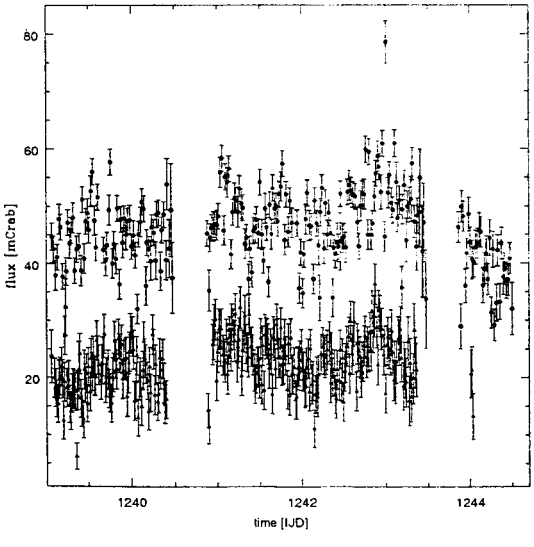

Fig. 3.— *INTEGRAL* ISGRI (circles, 2000 sec binning) and JEM-X2 (triangles, 1000 sec binning) lightcurve in the same energy bands as in Fig. 1.

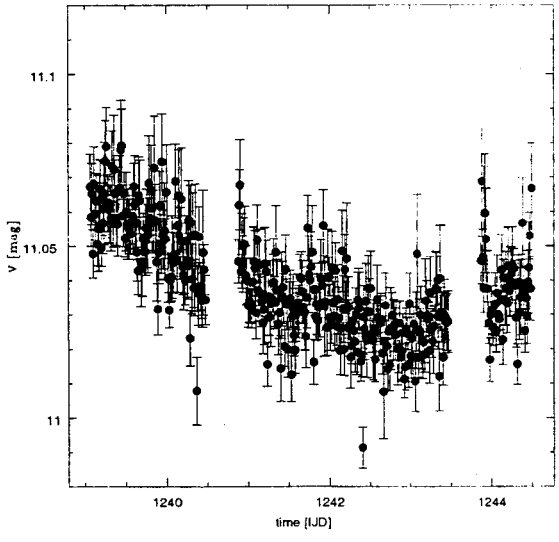

Fig. 4.— *INTEGRAL*/OMC light curve. Error bars are 1σ values.

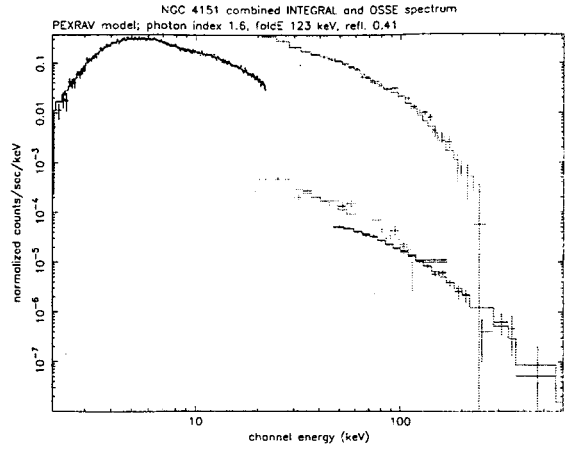

Fig. 5.— *INTEGRAL* and *CGRO*/OSSE simultaneous data fit. The OSSE data represent the average of the NGC 4151 spectra. All data are well represented by a PEXRAV model, with the individual OSSE data scaling with 0.6 ... 1.2 versus the *INTEGRAL*/JEM-X2 data.

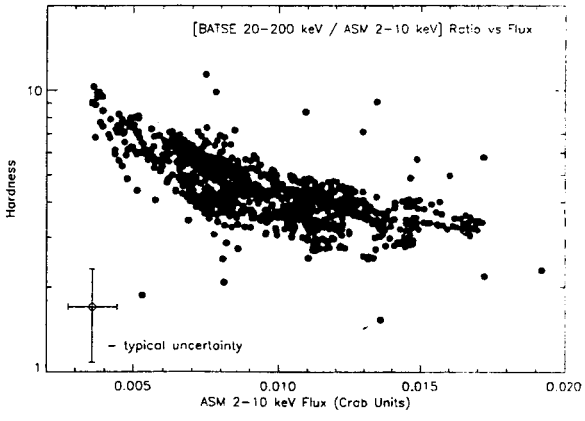

Fig. 6.— Spectral hardness derived from the BATSE and RXTE data, versus the *RXTE*/ASM flux. A softer spectrum is correlated with a higher flux. The error bars on the lower left show the typical uncertainties of the measurements.